



## OPEN ACCESS

## EDITED BY

Federico Rossi,  
Dipartimento d'Ingegneria, Università degli  
Studi di Perugia, Italy

## REVIEWED BY

Abdul Rehman Soomro,  
University of Perugia, Italy  
Mohamed Farahat,  
Faculty of engineering, Menoufia University,  
Egypt  
Luca Brunelli,  
Dipartimento d'Ingegneria, Università degli  
Studi di Perugia, Italy

## \*CORRESPONDENCE

Marc Medrano,  
✉ marc.medrano@udl.cat

RECEIVED 10 October 2025

REVISED 02 December 2025

ACCEPTED 25 December 2025

PUBLISHED 12 January 2026

## CITATION

Monterrubio J, Vilà R, Medrano M, Martorell I  
and Castell A (2026) Mapping radiative cooling  
potential for africa under different climate  
change scenarios.  
*Front. Environ. Sci.* 13:1722292.  
doi: 10.3389/fenvs.2025.1722292

## COPYRIGHT

© 2026 Monterrubio, Vilà, Medrano, Martorell  
and Castell. This is an open-access article  
distributed under the terms of the [Creative  
Commons Attribution License \(CC BY\)](#). The use,  
distribution or reproduction in other forums is  
permitted, provided the original author(s) and  
the copyright owner(s) are credited and that the  
original publication in this journal is cited, in  
accordance with accepted academic practice.  
No use, distribution or reproduction is permitted  
which does not comply with these terms.

# Mapping radiative cooling potential for africa under different climate change scenarios

Jesús Monterrubio, Roger Vilà, Marc Medrano\*, Ingrid Martorell and Albert Castell

Sustainable Energy, Machinery and Buildings (SEMB) Research Group, INSPIRES Research Centre, Universitat de Lleida, Lleida, Spain

Africa, with a significant portion of its territory located within the tropical latitudes, experiences high cooling demands. Addressing these requirements in a renewable way is possible thanks to Radiative Cooling (RC). RC utilizes the atmospheric window from 8 to 13  $\mu\text{m}$  to emit radiation to outer space, enabling the achievement of sub-ambient temperatures. A Kriging geospatial interpolation method is applied in this work to develop maps of RC potential, considering broadband emitters, for the typical meteorological year from 1991 to 2010 and predictions for 2030–2050 based on future emissions scenarios of the Intergovernmental Panel on Climate Change. A comparison is made between nighttime and all-day RC potential. The results reveal that all-day RC power potential is at least 22% higher than nighttime potential, while in terms of energy, the difference exceeds 156%. No significant variation is observed among future emissions scenarios. The average nighttime RC power potential exceeds 70  $\text{W}\cdot\text{m}^{-2}$ , while the average all-day potential surpasses 87  $\text{W}\cdot\text{m}^{-2}$ . Mean values for the nighttime RC energy potential are above 294  $\text{kWh}\cdot\text{m}^{-2}$ , while all-day results are over 763  $\text{kWh}\cdot\text{m}^{-2}$ . The potential of RC in many regions of Africa is promising and these maps will be a useful resource to estimate this RC potential.

## KEYWORDS

Africa, climate change, kriging, mapping, radiative cooling, renewable energy

## 1 Introduction

The residential and commercial sectors account for a 40% of global energy consumption (Atmaca and Atmaca, 2022). To align with the Green Deal (European commission, 2023), covering the thermal energy requirements of these spaces with renewable sources is essential. According to Alhuyi Nazari et al. (2023), the use of heat pumps has been widely adopted lately, regarding their good performance in terms of energy consumption and environmental impact. Despite the improvements in the heat pumps' coefficient of performance (COP), they still consume a significant amount of electricity. This makes it necessary to explore options with negligible or significantly low electric consumption.

Based on the prediction of a report by the International Energy Agency (The Future of Cooling, 2018), the energy demand for cooling is expected to experience a threefold increase by 2050, if no action is taken. This increase will be even more significant in Asian and African countries (The Future of Cooling, 2018). As the use of systems to meet cooling demands increases, such as heat pumps, there is also a rise in anthropogenically produced gas emissions that enhances climate change. Shi et al. estimate that the direct emissions of gaseous refrigerants will cause 45% of the greenhouse gas emissions by 2050 (Shi et al.,

2019), thus they are considered a threat to the planet (Sustain Innov Forum, 2015). Therefore, if polluting energy sources continue to be used, the situation can become cyclical.

A renewable alternative to meet the cooling demands is Radiative Cooling (RC), a strategy that enables cooling with a negligible consumption of electricity (Raman et al., 2014). This phenomenon utilizes the substantial transparency of the atmosphere within the infrared (IR) longwave spectral band, specifically from 8 to 13  $\mu\text{m}$  (atmospheric window) (Vall and Castell, 2017). By harnessing this optical attribute, RC effectively leverages the high transparency of the atmosphere to reject radiation to the space, thereby facilitating the attainment of temperatures below the ambient level through sustainable means.

## 1.1 Recent advances in RC materials

Previously, RC was limited to nighttime due to the low reflectivity of surface emitters in the solar spectrum. The energy balance on the radiator surface resulted in heating during the day and cooling when the Sun is not present. Recent advances in photonic, organic and metamaterial surfaces now enable daytime RC (Zhao et al., 2019; Su et al., 2023; Hossain et al., 2015; Cheng et al., 2025; Park et al., 2025). Multiple researchers have already achieved sub-ambient cooling during the day, thanks to proper material selection (Raman et al., 2014; Hwang, 2024; Ao et al., 2019; Li N. et al., 2019; Zhang et al., 2021; Han et al., 2022).

New materials are being developed with properties which are near the optimum for RC purposes. Raman et al. (2014) introduced a photonic solar reflector and thermal emitter that reflects 97% of incident sunlight, enabling temperatures 4.9 °C below ambient air temperature under direct sunlight. Han et al. (2022) used a polymeric coating with 97% solar reflectivity and 94.2% IR emissivity, maintaining surfaces below ambient temperature in tropical daytime. Zhai et al. (2017) developed a metamaterial transparent to the solar spectrum with 93% infrared emissivity. More recently, Cai et al. (2023) developed a cellulose nanocrystal aerogel grating with 94% infrared emissivity and 97.4% solar reflectivity. Song et al. (2023) developed a membrane made of porous thermoplastic urethanes with a thermal emissivity of 95% and solar reflectivity of 93%. Lin et al. (2023) developed a passive cooling ceramic with a near-perfect solar reflectivity (99.6%) and high thermal emissivity. The material proposed by Kang et al. (2025) achieved solar reflectance of 96.7% and emissivity of 94.5% in the atmospheric window range. Wang et al. (2024) reviewed daytime radiative cooling materials and their real-world applications. Liu et al. (2024) designed a thin paint with a solar reflectivity of 96.3% and longwave IR emissivity of 92.7%. Anson Tsang et al. (2024) developed a porous polymer bilayer with near-ideal solar reflectivity (over 99%) and blackbody-like longwave infrared emissivity of approximately 98% near normal incidence and 96% hemispherical.

In addition to academy, several companies have begun commercializing RC materials. For instance, Chillskyn™ (PDR, 2023) offers a polymer-based coating with a solar reflectivity of 96% and an infrared emissivity of 97%, while Spacecool (SPACECOOL Inc., 2023), has developed a multi-layered structure with a solar reflectivity exceeding 95% and infrared emissivity above 95%. Although RC materials are typically non-biodegradable, biomass-

based alternatives already exist, promoting sustainable development (Jia et al., 2025). With the availability of suitable materials, the combination of daytime and nighttime RC maximizes the daily cooling production.

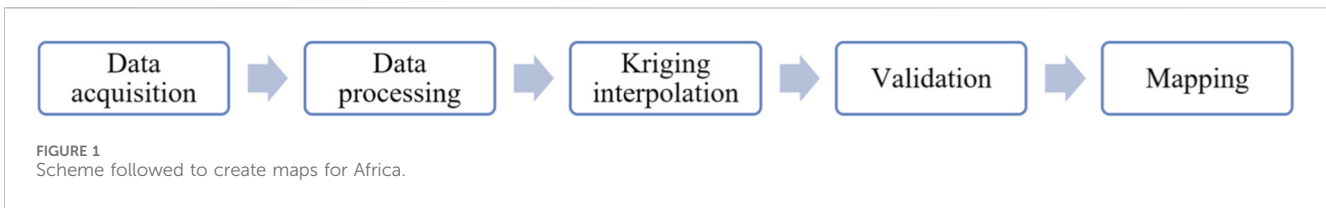
## 1.2 Mapping the potential of RC

Just as global solar atlas (Global Solar Atlas, 2023) provides information about solar radiation in different regions, recent developments have led to the creation of RC potential maps. These maps allow the determination of the maximum cooling power and energy that could be achieved using the RC phenomenon in a specific place. They are a powerful tool when deciding a suitable location for implementing the RC technology.

It is noteworthy that Argiriou et al. (1992) concluded that RC demonstrated successful applicability in the majority of locations in southern Europe. A more recent investigation found that Europe had its maximum RC power in the south, near Africa (Vilà et al., 2023). In fact, the map depicting the potential of annual average all-day RC, developed by Aili et al. (2021), reveals that the regions exhibiting the highest potential are situated in Northern Africa and the western region of Asia. Remarkably, within these geographical locations, the average potential exceeds the one observed in other global regions twofold.

Vilà et al. (2021) obtained mean values for the nighttime RC potential in Europe of  $47.30 \text{ W}\cdot\text{m}^{-2}$ , while mean values of  $60.17 \text{ W}\cdot\text{m}^{-2}$  were achieved with all-day RC. The average all-day RC power of China was above  $40 \text{ W}\cdot\text{m}^{-2}$ , according to Zhu et al. (2021). Chen et al. (2021) showed mean values of daytime RC in northwest China of  $60.10 \text{ W}\cdot\text{m}^{-2}$ . On the other hand, the United States achieved mean nighttime values of  $48.30 \text{ W}\cdot\text{m}^{-2}$ , according to the study conducted by Li and Coimbra (Li M. et al., 2019). Regarding the research conducted by Farooq et al. (2023), the Gulf Corporation Council (GCC) region exhibited a mean nighttime RC power of  $92.74 \text{ W}\cdot\text{m}^{-2}$ , while the mean daytime RC power decreased to  $67.77 \text{ W}\cdot\text{m}^{-2}$ .

Given that Africa occupies a substantial portion of the tropical area, and cooling demands remain generally high throughout the year, RC technology may play a crucial role in meeting these demands. Although global RC maps have been developed, Africa has not been analyzed in detail, and neither its future feasibility under different climate change scenarios has been assessed. The improvement of the RC potential in Africa, achieved throughout the day compared to nighttime, has not been investigated either. Therefore, unlike previous studies that focused on Europe or provided global averages, this work is the first to evaluate the RC potential in Africa under present and future climate scenarios. By applying geostatistical interpolation, all-day and nighttime RC power and energy potential are analyzed, extending the research conducted by Vilà et al. (2023) to Africa. Maps are presented for a hypothetical year which represents an average year of the period from 1991 to 2010 (typical meteorological year, TMY). Hereafter, current TMY refers to this period. All-day RC power potential maps with predictions for the years 2030, 2040, and 2050 are also presented with the aim of showing how the potential for applying RC in Africa will evolve in the coming decades. For each prediction, three different IPCC (Intergovernmental Panel



on Climate Change) scenarios are shown, allowing a more detailed analysis. These potential maps reflect the upper-bound cooling power achievable for sub-ambient applications under ideal conditions.

## 2 Methodology

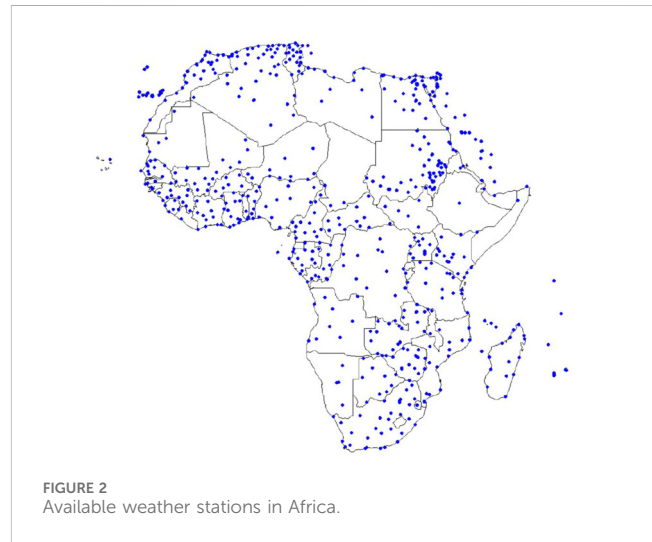
Different methodologies have been used for interpolating RC data. Some authors have used Inverse Distance Weighted (IDW) (Chen et al., 2021; Li M. et al., 2019), while others have applied Kriging (Vilà et al., 2023; Vilà et al., 2021; Zhu et al., 2021). Both approaches are suitable for generating spatial maps. However, Vilà et al. (2020) conducted a comparative analysis between IDW and Kriging. After cross-validation, the authors concluded that better results were obtained with Kriging interpolation, rather than with IDW. Therefore, in this work, we used Kriging to predict the power and the energy potential of RC in Africa.

Figure 1 illustrates the main steps followed in this research, based on (Vilà et al., 2023). Initially, for each year and its respective predictive scenario, we downloaded climate files from all available stations in Africa. Subsequently, we performed data processing to apply the stochastic interpolation method for RC power, RC energy, temperature, relative humidity, and atmospheric infrared radiation. Once all results were available, we validated them and plotted the charts and maps under analysis. The procedure is further detailed below.

### 2.1 Data acquisition

We downloaded meteorological data from Meteonorm v7.3.4 (Remund et al., 2019). The weather file contained multiple meteorological data recorded on an hourly basis. These data included dry bulb temperatures, relative humidities, global horizontal solar radiations, clearness index, atmospheric pressure and horizontal IR radiations.

It should be noted that the infrared radiation emitted by the sky ( $q_{sky}$  [ $W \cdot m^{-2}$ ]) was calculated by Meteonorm using the Aubinet model (Aubinet, 1994) (Equation 1). This model is also valid with broadband emitters, which are the type of materials considered in this article for generating the potential maps. Li et al. (2017) presented updated correlations, validated using experimental data only from North America. Although the Aubinet model was proposed in 1994, the review by Yan et al. (2024) suggests it, as an option that accounts for the ratio of extra-terrestrial radiation to global solar radiation and the clearness index. Therefore, we have opted to use the values provided by Meteonorm, as did by Vilà et al. (2023) for Europe.



$$q_{sky} = \sigma [94 + 12.6 \cdot \log(100 \cdot e_s) - 13 \cdot KT_d + 0.341 \cdot T_a]^4 \quad (1)$$

Where  $\sigma$  is the Stefan-Boltzmann constant [ $W \cdot m^{-2} \cdot K^{-4}$ ],  $e_s$  is the saturated vapor pressure [ $hPa$ ],  $KT_d$  is the clearness index [-] and  $T_a$  is the ambient temperature [ $K$ ].

The global horizontal solar radiation ( $q_{sun}$  [ $W \cdot m^{-2}$ ]) was calculated from the extraterrestrial horizontal solar radiation ( $q_{sun_0}$  [ $W \cdot m^{-2}$ ]) using the clearness index (Equation 2).

$$q_{sun} = KT_d \cdot q_{sun_0} \quad (2)$$

In Figure 2, the meteorological stations of Africa which were accessible through the weather data acquisition software are highlighted in blue. We downloaded a total amount of 610 weather files and formatted them with RStudio (version 2023.03). Nocturnal values were filtered when required for the obtention of nighttime results.

It is worth noting that there are more weather stations near big cities than in rural regions. An example of this is the case of the Sahara area, where few stations are available. This distribution may condition the results obtained with the interpolation procedure.

### 2.2 Data processing

Equation 3 allows the obtention of RC power potential ( $q_{RC}$  [ $W \cdot m^{-2}$ ]). This value reflects the heat exchange from the system to be cooled with RC (in transient state is not zero). The first term refers to the infrared radiation emitted by the surface to the atmosphere (Stefan-Boltzmann law), the second term accounts for the part of the atmosphere infrared radiation absorbed by the

surface and the third term refers to the solar radiation ( $q_{sun} [W \cdot m^{-2}]$ ) absorbed by the surface.

$$q_{RC} = \epsilon_s \sigma T_a^4 - \alpha_s q_{sky} - \alpha_{sun} q_{sun} \tag{3}$$

Where  $\epsilon_s$  is the emissivity of the RC surface [-],  $\alpha_s$  is the infrared absorptivity of the RC surface [-] and  $\alpha_{sun}$  is the solar absorptivity of the RC surface [-].

The following assumptions are made to determine the power potential, that is to say, the maximum power reachable under idealized conditions. This theoretical maximum provides a reference point for the best-case scenario.

- The surface temperature is considered equal to the ambient temperature. With this assumption, there are no conduction and convection losses, thereby maximizing the power potential.
- Maximum infrared absorptivity of the surface ( $\alpha_s = 1$ ), considering broadband emitters which behave like black bodies across the mid-infrared wavelength range, allowing for higher cooling powers compared to selective materials (Hu et al., 2016).
- Maximum infrared emissivity of the surface ( $\epsilon_s = 1$ ), according to the Kirchhoff Law ( $\alpha_s = \epsilon_s$ ).
- Maximum reflectivity of the surface to the solar radiation ( $\rho_{sun} = 1$ ). According to Equation 4,  $\alpha_{sun} = 0$ . It should be noted that, although the objective of this research is to determine the maximum potential of radiative cooling, there are already existing materials with properties very close to this optimal value, as discussed in the introduction section (Raman et al., 2014; Zhai et al., 2017; Cai et al., 2023; Song et al., 2023; Lin et al., 2023; Kang et al., 2025; Wang et al., 2024; Liu et al., 2024; Anson Tsang et al., 2024; PDRC, 2023; SPACECOOL Inc., 2023).

$$\alpha_{sun} = 1 - \rho_{sun} - \tau_{sun} \tag{4}$$

Where  $\tau_{sun}$  is the solar transmissivity of the RC surface [-].

From all the cooling potential values ( $q_{RC}$ ), the positive ones were filtered ( $q_{RC,p} [W \cdot m^{-2}]$ ), as negative values meant heating. Mean annual values were obtained with Equation 5, where  $n_p$  is the number of positive values of cooling power.

$$q_{RC,year} = \frac{\sum_{i=1}^{n_p} q_{RC,p_i}}{n_p} \tag{5}$$

The maximum annual achievable energy ( $e_{RC,year} [kWh \cdot m^{-2}]$ ) was calculated with Equation 6, where  $q_{RC,p_i}$  is the RC power potential for each hour and  $\Delta t$  is 1 h.

$$e_{RC,year} = \sum_{i=1}^{n_p} q_{RC,p_i} \cdot \Delta t \cdot 10^{-3} \tag{6}$$

### 2.3 Kriging interpolation

We generated a grid comprising 500,000 points to implement the spatial interpolation technique across the entire continent. Kriging interpolation considered all points with known data to estimate the 500,000 points distributed along Africa. With this methodology, points which are closer tend to have more similar

values than points which are more distant. Points which are clustered together carry less individual weight compared to isolated points located at the same distance (Webster and Oliver, 2007).

We followed the same methodology as previously conducted by Vilà et al. (2021). Two subgroups were created randomly: 80% of the available meteorological data were used to build the Kriging model, while the remaining 20% were used in the evaluation of the performance of the interpolation.

Firstly, the variogram was utilized to establish the spatial covariance structure of the available points. Selecting the appropriate mathematical models which best fit each variogram was essential to minimize the error (further details on the variogram are presented in Supplementary Tables A1, A2). Secondly, based on the weights derived from the covariance structure, values were interpolated for unobserved points across Africa.

In a general way, we estimated the unknown values ( $\hat{Z}(s_0)$ ) for each desired point of the grid ( $s_0$ ) using Equation 7, where  $\lambda_i$  are the weights,  $z(s_i)$  are the known data and  $N$  is the number of points with available data (80% of the downloaded climatic information, that is to say, 488 points).

$$\hat{Z}(s_0) = \sum_{i=1}^N \lambda_i z(s_i) \tag{7}$$

As stated by Webster and Oliver (Webster and Oliver, 2007), to ensure unbiased estimations, the sum of the weights must equal 1 (Equation 8).

$$\sum_{i=1}^N \lambda_i = 1 \tag{8}$$

### 2.4 Validation of the interpolated results

As mentioned previously, to validate the model, we utilized 20% of the available locations with meteorological information. The closer the predicted values match the observed values, the better the model performs.

We also calculated the coefficient of determination ( $R^2$ ) and the root mean square error (RMSE) using Equations 9, 10, respectively.

$$R^2 = \frac{\sum_{i=1}^M (x_{pred_i} - x_{obs_i})^2}{\sum_{i=1}^M (x_{obs_i} - \mu_i)^2} \tag{9}$$

$$RMSE = \sqrt{\frac{\sum_{i=1}^M (x_{pred_i} - x_{obs_i})^2}{M}} \tag{10}$$

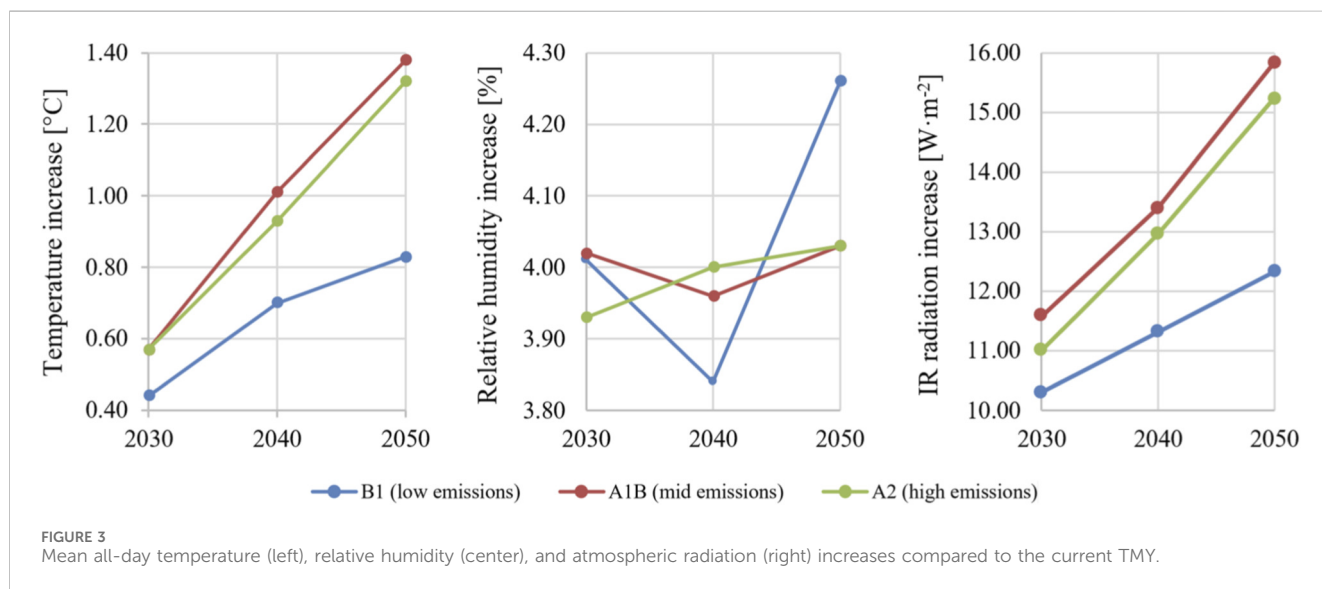
Where  $x_{pred_i}$  and  $x_{obs_i}$  are the predicted and observed values, respectively.  $\mu_i$  is the arithmetic mean of the observed samples and  $M$  represents the number of accessible data points (20% of the weather stations in Africa, 122 points).

### 2.5 Prediction scenarios

The three scenarios studied project a continuous rise in global mean surface air temperature (ambient temperature measured at a height of around 2 m). This temperature increase is mainly

TABLE 1 Temperature increase (°C) in 2090–2099 relative to 1980–1999.

Scenario	Emission level	Best estimate [°C]	Range of increase [°C]
B1	Low	1.8	1.1–2.9
A1B	Mid	2.8	1.7–4.4
A2	High	3.4	2.0–5.4



attributed to a rise in the concentration of anthropogenic greenhouse gases. The three different scenarios considered for the future predictions are based on the Fourth Assessment Report of the IPCC (Solomon et al., 2007). According to the report, the global mean temperature along with their uncertainty ranges are presented in Table 1. Scenarios B1, A1B, and A2 result from considering low, mid, and high emissions, respectively.

These scenarios have recently been replaced by the Shared Socioeconomic Pathways (SSPs) introduced in the IPCC’s Sixth Assessment Reports (Intergovernmental Panel on Climate Change IPCC, 2021). To ensure consistency, we link the scenarios used in this study to the more recent framework: B1 can be comparable to SSP2-4.5, A1B to SSP3-7.0 and A2 to SSP5-8.5.

### 3 Results and discussion

Figure 3 illustrates the projected average increases in temperature, relative humidity, and atmospheric radiation of Africa the coming years, based on the results of the interpolation method applied to the downloaded climate data files.

The lowest temperature increase is observed for scenario B1, as expected according to Table 1. Conversely, in the scenario A1B, the temperature increase is slightly higher than in A2. It is worth noting that the values in Table 1 refer to the period 2090–2099 relative to 1980–1999 and correspond to the mean world surface temperatures.

Therefore, it was expected to obtain different values for 2030–2050 relative to the current TMY in Africa.

Regarding relative humidity, no clear trend can be observed, as for different years, the maximum values are detected for different scenarios.

According to the model defined by Aubinet (1994), the infrared radiation emitted by the sky depends on the ambient temperature. An increase in radiation from the atmosphere is detected in all scenarios. The A1B scenario is projected to experience the greatest increase in atmospheric radiation, while the B1 scenario is expected to have the smallest increase. The difference between A1B and A2 scenarios is very low.

Mean annual values of all-day radiative cooling power and annual energy potentials are presented in the maps of Figure 4. The Sahara Desert, particularly Algeria, Niger, and the northern regions of Mali and Sudan exhibit the highest potential for RC. South Africa demonstrates a comparatively lower potential, but higher than what could be obtained in southern Europe (region of Europe with its maximum cooling power) (Vilà et al., 2021). The lowest results are observed along the western coast from Nigeria to Gabon. This tropical area is characterized by high temperatures and extremely high relative humidity, while the Sahara desert stands out for its high temperature and low relative humidity (Monterrubio et al., 2022). The energy map follows the same trend as the RC power potential map. The equivalent maps relative to nighttime radiative cooling are presented in the Supplementary Figure B1.

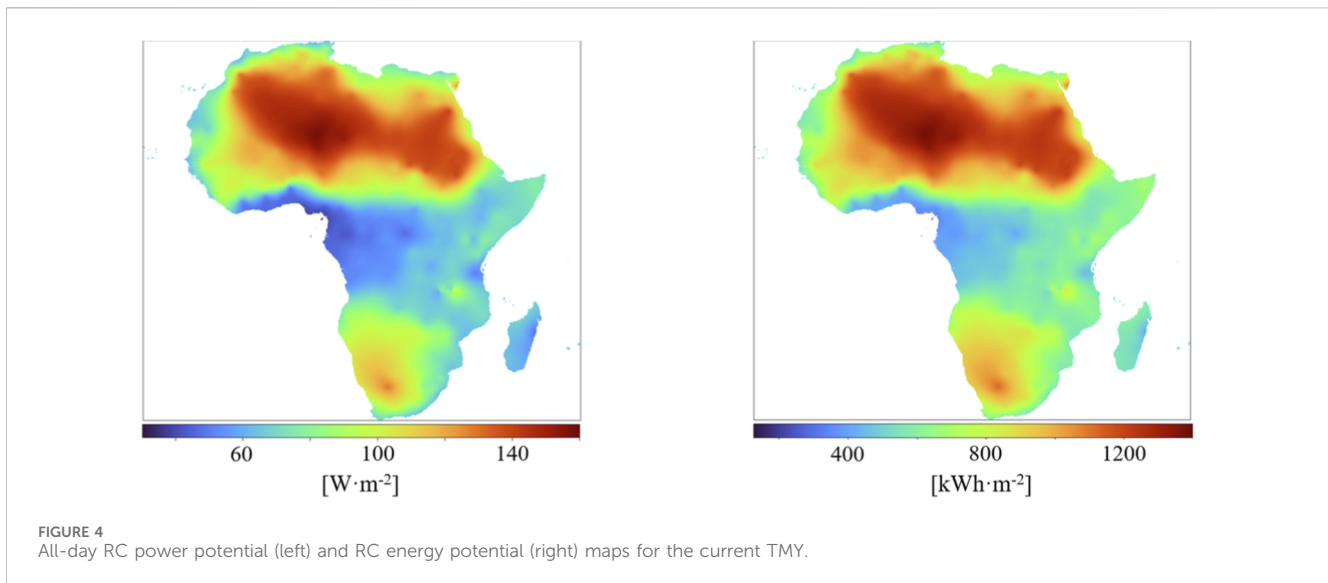


Figure 5 presents all-day RC maps for each of the analyzed scenarios for the years 2030, 2040, and 2050. Maps for nighttime RC power potential and energy are included in the Supplementary Figures B2, B3, while all-day RC energy potential maps can also be found in Supplementary Figure B4. Graphically, no significant differences are evident among the various scenarios or years. Comparing these maps with those in Figure 4, certain differences can be observed between the current TMY and future scenarios: both RC power and RC energy potentials are slightly lower. A more detailed discussion is presented later, based on the results from Tables 2, 3.

Tables 2, 3 include the extreme and mean values of both RC power and energy potentials for nighttime and all-day RC, respectively. The extreme values correspond to the highest and lowest values observed at specific locations within the entire map in the range 1990–2010, while the mean values show the average calculated across all locations for the same time period. It can be observed that the results are higher in the case of all-day RC. In the case of energy, the increase is even more pronounced, as the number of hours available for RC increases. In fact, the average RC power potential shows an increase of over 22% in all cases, while RC energy potential has an increase of over 156%.

The mean nighttime RC power potential exceeds  $70 \text{ W}\cdot\text{m}^{-2}$  in all the cases, while the mean all-day RC power potential surpasses  $87 \text{ W}\cdot\text{m}^{-2}$ , values higher than those reported for other countries and continents in the introduction section. Compared with the average reported RC power potential results for Europe (Vilà et al., 2023), a continent close to Africa, the nighttime RC values in Africa exceed those of Europe by over 45%, while for all-day RC, they surpass Europe by over 51% (see Table 4).

As previously discussed, the most significant change is observed between the current TMY and the projected values for 2030, whereas the subsequent years present less noticeable variations and remain stable. The maximum values are higher for the current TMY than for the predictions, while the minimum values are lower (see Tables 2, 3).

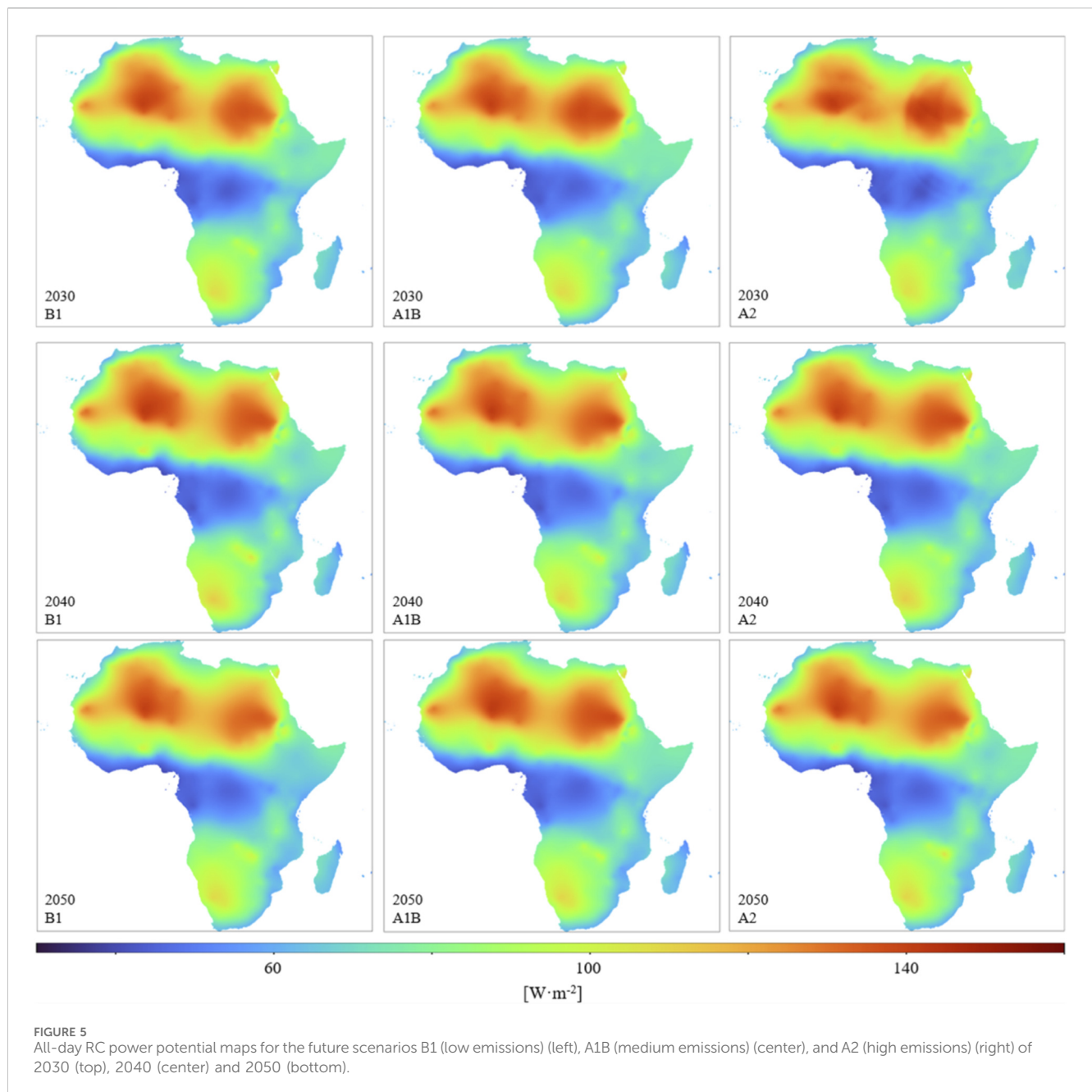
Although average temperatures increase compared to the current TMY, RC power potentials decrease. The balance to

obtain  $q_{RC}$  gives lower results for future emissions scenarios (see columns  $\Delta\text{Mean}$  from Tables 2, 3 regarding RC power potential). This can be explained by the increase in atmospheric IR radiation. The radiation emitted by the surface increases due to the higher temperature. However, the radiation from the atmosphere is even greater, resulting in a slight reduction in the RC power potential (Figure 6). Vilà et al. reported similar findings in their study conducted in Europe (Vilà et al., 2023).

Despite having the values for each scenario, none of them exhibits the best results for all years. This is because the relative humidity does not follow a clear pattern during the analyzed period (Figure 3). However, differences among scenarios are negligible, well below the errors (RMSE) obtained for the predicting model (see Table 5).

Table 5 summarizes the metrics used to evaluate the models created for the interpolation. All interpolations show  $R^2$  values higher than 0.73 for both RC power potential and RC energy potential. The RMSE values are lower than  $10.78 \text{ W}\cdot\text{m}^{-2}$  for RC power potential. Since the values of energy vary significantly depending on whether it is nighttime RC or all-day RC, the RMSE values are also significantly different. For nighttime RC energy potential, RMSE does not exceed  $44.91 \text{ kWh}\cdot\text{m}^{-2}$  in any case, while for all-day RC energy potential, the maximum is found for 2030-A1B, with  $98.94 \text{ kWh}\cdot\text{m}^{-2}$ . These values represent less than 15.5% of the mean power and energy potentials results (in most cases less than 13%), which is acceptable considering that there are places with scarce available data.

It should be noted that the best metrics are achieved for the current TMY, with  $R^2$  values above 0.94. Certain regions lack meteorological data (Figure 2), which combined with the predictions made by Meteonom, can explain the difference between the metrics for the current TMY and future years. This trend can also be observed in (Supplementary Figures A1, A3), which present scatter plots comparing predicted and observed RC power potential values. Each plot includes a red reference line representing perfect agreement. The closer the points lie to the line, the better the model's performance. In future scenarios, the



scatter plots show larger deviations from the reference line, consistent with lower  $R^2$  and higher RMSE values.

We have summarized the RC power potential results obtained for different parts of the world (see Table 6). A significant increase in cooling power potential is observed in United States (over 9%), Europe (over 19%) and Africa (over 22%) by applying RC throughout the day, not just during the night. Therefore, Africa not only has a higher average RC power, but also presents greater potential for enhancement in the implementation of daytime RC, using the new materials under development.

The cooling power is higher for nighttime RC ( $92.74 \text{ W}\cdot\text{m}^{-2}$ ) than for daytime RC ( $67.77 \text{ W}\cdot\text{m}^{-2}$ ) across the Gulf Corporation Council region. This is because Farooq et al. (2023), unlike the other authors, considered non-ideal optical properties for the material

used to model the RC power maps (94% reflectivity within the ultraviolet to near-infrared range, 98% reflectivity within the visible range and 97% emissivity within the main atmospheric window). Thus, although the all-day mode includes more available hours for cooling, solar radiation incidence can cause heating instead of cooling in some cases.

Additionally, Africa is distinguished by its high cooling potential compared to the other locations. Not only in Africa but also in Europe, the RC power potential remains stable over the years.

The high cooling power potential in Africa is motivated by its meteorological conditions, characterized by high mean temperatures (Supplementary Figures C1–C3) and low relative humidity (Supplementary Figures C4–C6) in the regions with maximum cooling performance. Although

TABLE 2 Annual average nighttime RC power and energy potentials for different years and scenarios.

Year	Scenario	RC power potential [W·m <sup>-2</sup> ]			RC energy potential [kWh·m <sup>-2</sup> ]				
		Min	Max	Mean	ΔMean <sup>a</sup>	Min	Max	Mean	ΔMean <sup>a</sup>
Current TMY	-	31.35	135.80	77.64	-	128.97	558.45	324.88	-
2030	B1	33.05	119.12	70.63	-7.01	136.69	496.62	296.23	-28.65
	A1B	33.58	120.43	70.85	-6.79	139.08	501.71	297.21	-27.67
	A2	32.17	122.18	70.07	-7.57	132.26	510.35	294.00	-30.88
2040	B1	34.18	117.48	70.63	-7.01	142.98	491.83	297.16	-27.72
	A1B	33.98	118.01	70.71	-6.93	139.44	492.21	297.47	-27.41
	A2	33.87	118.72	70.43	-7.21	140.46	496.94	296.32	-28.56
2050	B1	30.53	122.16	70.33	-7.31	125.53	509.83	295.11	-29.77
	A1B	33.03	116.89	70.27	-7.37	136.57	488.19	294.88	-30.00
	A2	32.70	118.74	70.69	-6.95	135.35	496.17	296.62	-28.26

<sup>a</sup>Variation of the mean value for each year and scenario with respect to the current TMY (negative values indicate reduction).

TABLE 3 Annual average all-day RC power and energy potentials for different years and scenarios.

Year	Scenario	RC power potential [W·m <sup>-2</sup> ]			RC energy potential [kWh·m <sup>-2</sup> ]				
		Min	Max	Mean	ΔMean <sup>a</sup>	Min	Max	Mean	ΔMean <sup>a</sup>
Current TMY	-	39.13	157.15	94.95	-	342.74	1376.62	831.79	-
2030	B1	41.82	140.22	87.46	-7.49	366.31	1228.31	766.17	-65.62
	A1B	41.86	140.34	87.57	-7.38	366.68	1229.37	767.12	-64.67
	A2	41.11	142.07	87.36	-7.59	360.11	1244.50	765.27	-66.52
2040	B1	40.57	141.97	87.78	-7.17	356.37	1247.06	771.05	-60.74
	A1B	41.02	141.51	87.46	-7.49	360.31	1243.03	768.26	-63.53
	A2	40.86	140.42	87.52	-7.43	358.93	1233.43	768.75	-63.04
2050	B1	40.67	140.40	87.18	-7.77	356.27	1229.94	763.70	-68.09
	A1B	41.20	141.60	87.83	-7.12	360.92	1240.43	769.39	-62.40
	A2	40.22	141.04	87.39	-7.56	352.35	1235.50	765.57	-66.22

<sup>a</sup>Variation of the mean value for each year and scenario with respect to the current TMY (negative values indicate reduction).

TABLE 4 Percentages of increase of the mean annual RC power potential of Africa with respect to Europe.

RC working mode	2030			2040			2050		
	B1	A1B	A2	B1	A1B	A2	B1	A1B	A2
Nighttime (%)	46.90	47.60	45.49	47.39	47.31	46.58	46.77	47.29	47.89
All-day (%)	52.00	52.75	51.82	52.74	52.32	52.39	51.72	53.33	52.67

temperatures are expected to rise in the future, the atmospheric radiation is also expected to increase (Figure 3), leading to the slight reduction observed in the predicted values presented in the previous table.

Beyond the cooling potential, the connection with actual cooling needs in populated areas should be considered. Previous studies have indicated that the applicability of

radiative cooling depends not only on weather conditions but also on population density and building demand. Aili et al. (2021) developed global maps and found that areas with moderate population density are particularly suitable for RC application, while Vilà et al. (2025) analyzed European data and demonstrated that daytime RC can partially meet building cooling requirements depending on climate and building characteristics. In the African

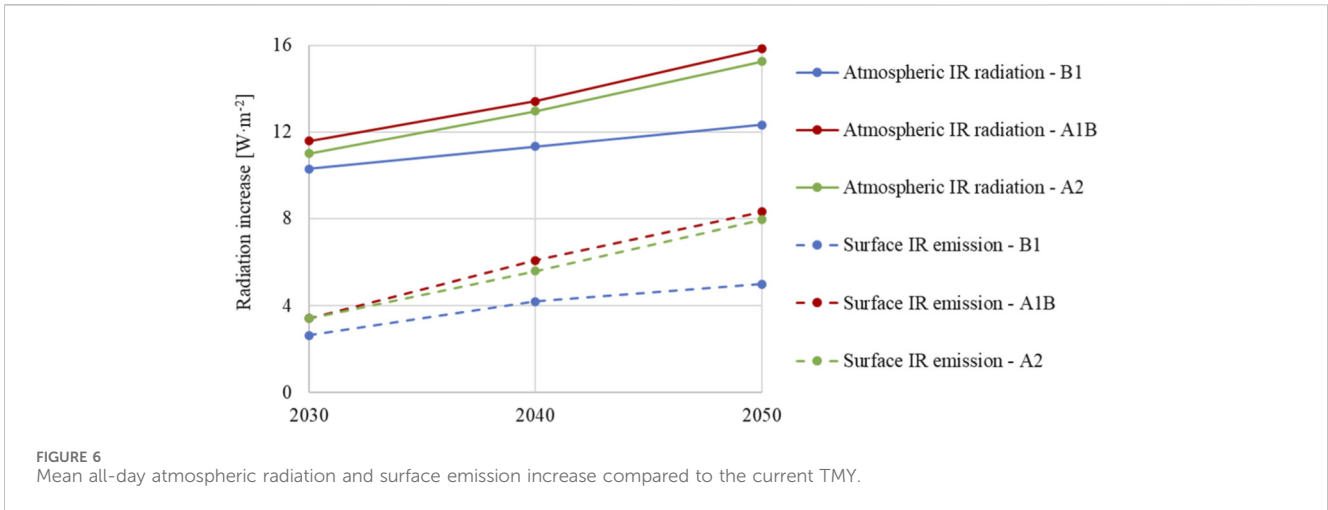


FIGURE 6 Mean all-day atmospheric radiation and surface emission increase compared to the current TMY.

TABLE 5 Metrics for the models' performance assessment.

Year	Scenario	Nighttime				All-day			
		RC power potential		RC energy potential		RC power potential		RC energy potential	
		$R^2$	RMSE [ $Wm^{-2}$ ]	$R^2$	RMSE [ $kWhm^{-2}$ ]	$R^2$	RMSE [ $Wm^{-2}$ ]	$R^2$	RMSE [ $kWhm^{-2}$ ]
Current TMY	-	0.96	4.72	0.96	19.58	0.94	7.14	0.94	62.57
2030	B1	0.75	10.21	0.75	42.66	0.83	10.12	0.83	88.68
	A1B	0.79	9.58	0.79	40.04	0.79	11.29	0.79	98.94
	A2	0.73	10.78	0.73	44.91	0.82	10.22	0.82	89.55
2040	B1	0.79	9.40	0.79	39.57	0.82	10.33	0.82	90.70
	A1B	0.79	9.53	0.79	39.94	0.79	11.17	0.79	98.09
	A2	0.80	9.22	0.80	38.79	0.81	10.70	0.81	93.97
2050	B1	0.77	9.95	0.77	41.41	0.82	10.25	0.82	89.83
	A1B	0.78	9.71	0.78	40.49	0.82	10.35	0.82	90.63
	A2	0.75	10.39	0.75	43.39	0.82	10.35	0.82	90.67

context, RC may have greater relevance in regions with significant cooling needs and dense population, rather than in remote regions with limited demand, despite having higher cooling potential. Consequently, although the Sahara Desert exhibits the maximum RC power potential, its practical relevance is limited by the low population density.

### 4 Conclusions

As seen in the previous section, several authors are working on determining the radiative cooling potential in different locations. In this study, we have mapped the RC power and RC energy potentials for Africa, a continent which shows great potential in the implementation of RC technology because of its geoclimatic characteristics.

We have also included future projections, allowing further analysis on the effect of different climate change scenarios. Based on the results obtained, the following conclusions can be derived.

- The predictive models used with Kriging interpolation are reliable, as good metrics have been obtained. The results for all-day RC demonstrate better performance than those of nighttime RC.
- The maximum RC power potential is observed in the northern region, particularly around the Sahara desert, where power peaks of  $157.15 W \cdot m^{-2}$  and annual cooling productions up to  $1376.62 kWh \cdot m^{-2}$  can be found with all-day RC.
- The minimum RC power potential is found over the western coastal countries of the tropical region. This part of Africa is characterized by high relative humidity, over 80%.
- There is a slight reduction in both RC power and energy potentials between the current TMY and the following years,

**TABLE 6** Comparison of the mean annual RC power across different regions of the world. Ranges of RC power potential are presented regarding different regions of China and different scenarios of Europe and Africa. "N/A" stands for "Not Available". "GCC" stands for "Gulf Corporation Council" region.

Source	Meteorological data year	Location	Average RC power [W·m <sup>-2</sup> ]	
			All-day/Day time	Night time
Chen et al. (2021)	2005 (TMY)	China	48.80–60.10	N/A
Zhu et al. (2021)	2005 (TMY)	China	40.00–55.00	N/A
Li N. et al. (2019)	2017	United States	52.70	48.30
Farooq et al. (2023)	N/A	GCC	67.77	92.74
Vilà et al. (2021)	Current TMY	Europe	60.17	47.30
Vilà et al. (2023)	2030	Europe	57.33–57.54	48.00–48.16
	2040	Europe	57.42–57.47	47.92–48.05
	2050	Europe	57.24–57.46	47.71–47.92
New contribution	Current TMY	Africa	94.95	77.64
	2030	Africa	87.36–87.57	70.07–70.85
	2040	Africa	87.46–87.78	70.73–70.71
	2050	Africa	87.18–87.83	70.27–70.69

with a decrease of less than 10%. No significant variation is detected among the different projections, which means that RC will be resilient to climate change in Africa and can be untapped as a robust renewable cooling technology at present and in the years to come.

- RC potentials in Africa are higher than those reported for Europe, China, and the United States of America (Table 6).

It is important to recognize the limitations of the present work, which could be addressed in future studies.

- Although the RMSE and R<sup>2</sup> values are adequate for the stochastic interpolation, limited meteorological data in sparsely populated regions reduces the accuracy of the results. A more uniform distribution of meteorological stations would improve interpolation performance.
- The Aubinet model used to estimate atmospheric radiation may introduce small biases, as it has not been validated in Africa. Using an atmospheric radiation model specifically validated for the African continent would increase confidence in the calculated values, but would not change the conclusions of this study.
- The assumption of broadband ideal materials at ambient temperature provides the maximum theoretical RC potential, which was the objective of this study. However, considering real broadband and selective materials at subambient or above ambient temperatures would yield values more representative of real-world applications.
- Population density was not considered in this study. Developing additional maps that integrate population distribution and cooling demand would allow to obtain results that better reflect the practical relevance of RC potential.

In conclusion, RC can play a significant role in the near future for providing renewable cooling in Africa. The RC potential in Africa for future scenarios remains higher than in other regions. The

maps presented in this article enable the estimation of renewable cooling production by means of radiative cooling in each specific zone of Africa. Beyond the technical results, the application of RC has clear policy relevance, because it contributes to some Sustainable Development Goals (SDGs): SDG 7 (Affordable and Clean Energy), SDG 11 (Sustainable Cities and Communities), and SDG 13 (Climate Action).

## Data availability statement

The raw data supporting the conclusions of this article will be made available by the authors, without undue reservation.

## Author contributions

JM: Conceptualization, Validation, Methodology, Data curation, Writing – original draft, Investigation, Formal Analysis, Visualization. RV: Writing – review and editing, Validation, Investigation, Methodology, Formal Analysis, Supervision, Conceptualization. MM: Resources, Conceptualization, Funding acquisition, Project administration, Writing – review and editing. IM: Project administration, Resources, Writing – review and editing, Supervision, Funding acquisition. AC: Investigation, Funding acquisition, Writing – review and editing, Formal Analysis, Resources, Supervision, Project administration, Conceptualization.

## Funding

The author(s) declared that financial support was received for this work and/or its publication. This publication is part of the grant PID2021-126643OB-I00, funded by MCIN/AEI/10.13039/501100011033/and by “ERDF A way of making Europe”. This

publication is part of the grant TED2021-131446B-I00, funded by MCIN/AEI/10.13039/501100011033/and by the “European Union NextGenerationEU/PRTR”. This publication is part of the grant PDC2022-133215-I00, funded by MCIN/AEI/10.13039/501100011033/and by the “European Union NextGenerationEU/PRTR”. The authors would like to thank Generalitat de Catalunya for the project awarded to their research group (2021 SGR 01370). JM would like to thank the grant FPU22/01304 funded by MICIU/AEI/10.13039/501100011033 and by “ESF+”.

## Conflict of interest

The author(s) declared that this work was conducted in the absence of any commercial or financial relationships that could be construed as a potential conflict of interest.

## Generative AI statement

The author(s) declared that generative AI was not used in the creation of this manuscript.

## References

- Sustain Innov Forum (2015). United nations framework convention on climate change. Paris Agreement. Available online at: <https://www.un.org/sustainabledevelopment/cop21/>
- Aili, A., Yin, X., and Yang, R. (2021). Global radiative sky cooling potential adjusted for population density and cooling demand. *Atmosphere* 12 (11), 1379. doi:10.3390/atmos12111379
- Alhuyi Nazari, M., Rungamornrat, J., Prokop, L., Blazek, V., Misak, S., Al-Bahrani, M., et al. (2023). An updated review on integration of solar photovoltaic modules and heat pumps towards decarbonization of buildings. *Energy Sustain. Dev.* 72, 230–242. doi:10.1016/j.esd.2022.12.018
- Anson Tsang, Y. C., Jo Varghese, N., Degeorges, M., and Mandal, J. (2024). Porous polymer bilayer with near-ideal solar reflectance and longwave infrared emittance. *Nanophotonics* 13 (5), 669–677. doi:10.1515/nanoph-2023-0707
- Ao, X., Hu, M., Zhao, B., Chen, N., Pei, G., and Zou, C. (2019). Preliminary experimental study of a specular and a diffuse surface for daytime radiative cooling. *Sol. Energy Mater. Sol. Cells* 191, 290–296. doi:10.1016/j.solmat.2018.11.032
- Argiriou, A., Santamouris, M., Balaras, C., and Jeter, S. (1992). Potential of radiative cooling in Southern Europe. *Int. J. Sol. Energy* 13 (3), 189–203. doi:10.1080/01425919208909784
- Atmaca, A., and Atmaca, N. (2022). Carbon footprint assessment of residential buildings, a review and a case study in Turkey. *J. Clean. Prod.* 340, 130691. doi:10.1016/j.jclepro.2022.130691
- Aubinet, M. (1994). Longwave sky radiation parametrizations. *Sol. Energy* 53 (2), 147–154. doi:10.1016/0038-092X(94)90475-8
- Cai, C., Chen, W., Wei, Z., Ding, C., Sun, B., Gerhard, C., et al. (2023). Bioinspired “aerogel grating” with metasurfaces for durable daytime radiative cooling for year-round energy savings. *Nano Energy* 114, 108625. doi:10.1016/j.nanoen.2023.108625
- Chen, J., Lu, L., and Gong, Q. (2021). A new study on passive radiative sky cooling resource maps of China. *Energy Convers. Manag.* 237, 114132. doi:10.1016/j.enconman.2021.114132
- Cheng, L., Chen, H., Cai, Q., Deng, J., Cheng, H., Fan, X., et al. (2025). Ultra-efficient passive daytime radiative cooling enabled by dual-selective inorganic SiO<sub>2</sub>/Si<sub>3</sub>N<sub>4</sub> photonic emitter. *Laser and Photonics Rev.* n/a (n/a), 2500068. doi:10.1002/lpor.202500068
- European commission (2023). A European green deal. (Accessed: June. 15, 2023). Available online at: [https://commission.europa.eu/strategy-and-policy/priorities-2019-2024/european-green-deal\\_en](https://commission.europa.eu/strategy-and-policy/priorities-2019-2024/european-green-deal_en)
- Farooq, A. S., Alkaabi, K., and Hdhaiba, S. B. (2023). Exploring radiative sky cooling resource map and the impact of meteorological conditions on radiative emitters. A perspective of GCC countries. *Energy Rep.* 10, 473–483. doi:10.1016/j.egy.2023.06.054
- Global Solar Atlas (2023). Global wind atlas (Accessed: June. 15, 2023). Available online at: <https://globalsolaratlas.info/map?c=11.523088,8.173828,3>.
- Han, D., Fei, J., Mandal, J., Liu, Z., Li, H., Raman, A. P., et al. (2022). Sub-ambient radiative cooling under tropical climate using highly reflective polymeric coating. *Sol. Energy Mater. Sol. Cells* 240, 111723. doi:10.1016/j.solmat.2022.111723
- Hossain, M. M., Jia, B., and Gu, M. (2015). A metamaterial emitter for highly efficient radiative cooling. *Adv. Opt. Mater.* 3 (8), 1047–1051. doi:10.1002/adom.201500119
- Hu, M., Pei, G., Wang, Q., Li, J., Wang, Y., and Ji, J. (2016). Field test and preliminary analysis of a combined diurnal solar heating and nocturnal radiative cooling system. *Appl. Energy* 179, 899–908. doi:10.1016/j.apenergy.2016.07.066
- Hwang, J. (2024). Daytime radiative cooling under extreme weather conditions. *Adv. Energy Sustain. Res.* 5 (5), 2300239. doi:10.1002/aesr.202300239
- Intergovernmental Panel on Climate Change (IPCC) (2021). *Climate change 2021: the physical science basis*. Cambridge, United Kingdom: Cambridge University Press.
- Jia, H., Zhang, J., Hou, Y., Pan, Y., Liu, C., Shen, C., et al. (2025). Bio-Mass radiative cooling materials: progress and prospects. *Adv. Sustain. Syst.* 9 (2), 2400773. doi:10.1002/adsu.202400773
- Kang, D.-C., Wang, T.-Y., Lin, D.-S., Cheng, Y.-S., and Huang, C.-W. (2025). PDMS with porous PMMA dual-layer coating for passive daytime radiative cooling. *Sol. Energy Mater. Sol. Cells* 282, 113380. doi:10.1016/j.solmat.2024.113380
- Li, M., Jiang, Y., and Coimbra, C. F. M. (2017). On the determination of atmospheric longwave irradiance under all-sky conditions. *Sol. Energy* 144, 40–48. doi:10.1016/j.solener.2017.01.006
- Li, N., Wang, J., Liu, D., Huang, X., Xu, Z., Zhang, C., et al. (2019). Selective spectral optical properties and structure of aluminum phosphate for daytime passive radiative cooling application. *Sol. Energy Mater. Sol. Cells* 194, 103–110. doi:10.1016/j.solmat.2019.01.036
- Li, M., Peterson, H., and Coimbra, C. (2019). Radiative cooling resource maps for the contiguous United States. *J. Renew. Sustain. Energy* 11, 036501. doi:10.1063/1.5094510
- Lin, K., Chen, S., Zeng, Y., Ho, T. C., Zhu, Y., Wang, X., et al. (2023). Hierarchically structured passive radiative cooling ceramic with high solar reflectivity. *Science* 382 (6671), 691–697. doi:10.1126/science.ad4725
- Liu, S., Zhang, F., Chen, X., Yan, H., Chen, W., and Chen, M. (2024). Thin paints for durable and scalable radiative cooling. *J. Energy Chem.* 90, 176–182. doi:10.1016/j.jechem.2023.11.016
- Monterrubio, J., Vilà, R., Castell, A., Rincón, L., and Martorell, I. (2022). “Mapping radiative cooling potential predictions for Africa,” in *EuroSun 2022 - ISES and IEA SHC international conference on solar energy for buildings and industry* (Germany: Kassel), 1–7.

Any alternative text (alt text) provided alongside figures in this article has been generated by Frontiers with the support of artificial intelligence and reasonable efforts have been made to ensure accuracy, including review by the authors wherever possible. If you identify any issues, please contact us.

## Publisher’s note

All claims expressed in this article are solely those of the authors and do not necessarily represent those of their affiliated organizations, or those of the publisher, the editors and the reviewers. Any product that may be evaluated in this article, or claim that may be made by its manufacturer, is not guaranteed or endorsed by the publisher.

## Supplementary material

The Supplementary Material for this article can be found online at: <https://www.frontiersin.org/articles/10.3389/fenvs.2025.1722292/full#supplementary-material>

- Park, J., Chae, D., Lim, H., Ha, J., Park, S., Sung, H., et al. (2025). Daytime radiative cooling sheet functionalized by Al<sub>2</sub>O<sub>3</sub>-Assisted organic composite. *Adv. Sci.* 12, 2417584. doi:10.1002/advs.202417584
- PDRC (2023). ChillSkyn solutions, ChillSkyn - PDRC (Accessed: July. 13, 2023). Available online at: <https://www.chillskyn.com>.
- Raman, A. P., Anoma, M. A., Zhu, L., Rephaeli, E., and Fan, S. (2014). Passive radiative cooling below ambient air temperature under direct sunlight. *Nature* 515 (7528), 540–544. doi:10.1038/nature13883
- Remund, J., Müller, S., Kunz, S., Huguenin-Landl, B., Studer, C., and Cattin, R. (2019). *Meteonorm*. Switzerland: Meteotest.
- Shi, J., Han, D., Li, Z., Yang, L., Lu, S. G., Zhong, Z., et al. (2019). Electrocaloric cooling materials and devices for zero-global-warming-potential, high-efficiency refrigeration. *Joule* 3 (5), 1200–1225. doi:10.1016/j.joule.2019.03.021
- Solomon, S., Qin, D., Manning, M., Chen, Z., Marquis, M., Averyt, K., et al. (2007). *IPCC, 2007: climate change 2007: the physical science basis. Contribution of working group I to the fourth assessment report of the intergovernmental panel on climate change* (Cambridge; New York: Cambridge University Press).
- Song, Y., Zhan, Y., Li, Y., and Li, J. (2023). Scalable fabrication of super-elastic TPU membrane with hierarchical pores for subambient daytime radiative cooling. *Sol. Energy* 256, 151–157. doi:10.1016/j.solener.2023.03.018
- SPACECOOL Inc. (2023). SPACECOOL. Tokyo, Japan: SPACECOOL. (Accessed: July. 13, 2023). Available online at: <https://spacecool.jp/en/>
- Su, W., Cai, P., Darkwa, J., Hu, M., Kokogiannakis, G., Xu, C., et al. (2023). Review of daytime radiative cooling technologies and control methods. *Appl. Therm. Eng.* 235, 121305. doi:10.1016/j.applthermaleng.2023.121305
- The Future of Cooling (2018). *The future of cooling. Opportunities for energy-efficient air-conditioning*. IEA.
- Vall, S., and Castell, A. (2017). Radiative cooling as low-grade energy source: a literature review. *Renew. Sustain. Energy Rev.* 77, 803–820. doi:10.1016/j.rser.2017.04.010
- Vilà, R., Rincón, L., Medrano, M., and Castell, A. (2020). “Radiative cooling potential maps for Spain,” in *Proceedings of the ISES EuroSun 2020 conference – 13th international conference on solar energy for buildings and industry* (Freiburg, Germany: International Solar Energy Society), 1–9. doi:10.18086/eurosun.2020.09.01
- Vilà, R., Medrano, M., and Castell, A. (2021). Mapping nighttime and all-day radiative cooling potential in Europe and the influence of solar reflectivity. *Atmosphere* 12 (9), 1119. doi:10.3390/atmos12091119
- Vilà, R., Medrano, M., and Castell, A. (2023). Climate change influences in the determination of the maximum power potential of radiative cooling. Evolution and seasonal study in Europe. *Renew. Energy* 212, 500–513. doi:10.1016/j.renene.2023.05.083
- Vilà, R., Casasnovas, A., and Castell, A. (2025). Exploring the suitability of radiative cooling: comparing daytime cooling production with cooling demand in buildings – A European perspective. *Energy Build.* 347, 116214. doi:10.1016/j.enbuild.2025.116214
- Wang, C., Chen, H., and Wang, F. (2024). Passive daytime radiative cooling materials toward real-world applications. *Prog. Mater. Sci.* 144, 101276. doi:10.1016/j.pmatsci.2024.101276
- Webster, R., and Oliver, M. A. (2007). *Geostatistics for environmental scientists*. John Wiley and Sons.
- Yan, T., Xu, D., Meng, J., Xu, X., Yu, Z., and Wu, H. (2024). A review of radiative sky cooling technology and its application in building systems. *Renew. Energy* 220, 119599. doi:10.1016/j.renene.2023.119599
- Zhai, Y., Ma, Y., David, S. N., Zhao, D., Lou, R., Tan, G., et al. (2017). Scalable-manufactured randomized glass-polymer hybrid metamaterial for daytime radiative cooling. *Science* 355 (6329), 1062–1066. doi:10.1126/science.aai7899
- Zhang, Y., Tan, X., Qi, G., Yang, X., Hu, D., Fyffe, P., et al. (2021). Effective radiative cooling with ZrO<sub>2</sub>/PDMS reflective coating. *Sol. Energy Mater. Sol. Cells* 229, 111129. doi:10.1016/j.solmat.2021.111129
- Zhao, B., Hu, M., Ao, X., Chen, N., and Pei, G. (2019). Radiative cooling: a review of fundamentals, materials, applications, and prospects. *Appl. Energy* 236, 489–513. doi:10.1016/j.apenergy.2018.12.018
- Zhu, Y., Qian, H., Yang, R., and Zhao, D. (2021). Radiative sky cooling potential maps of China based on atmospheric spectral emissivity. *Sol. Energy* 218, 195–210. doi:10.1016/j.solener.2021.02.050